The Role of Glycocalyx in Nanocarrier-Cell Adhesion Investigated using a Thermodynamic Model and Monte Carlo Simulations*

Neeraj J. Agrawal[1], Ravi Radhakrishnan[2,†]

[1] Chemical and Biomolecular Engineering, [2] Bioengineering, University of Pennsylvania, 240 Skirkanich Hall, 210 S. 33rd St, Philadelphia, PA 19104.

Abstract

We present an equilibrium model for quantifying the effect of glycocalyx in mediating the interaction of functionalized nanocarriers with endothelial cells. In this model, nanocarrier adhesion is governed by the interplay between three physical parameters, namely, glycocalyx resistance, flexural rigidity of receptors, and receptor-ligand bond-stiffness. We describe a procedure to rationally determine the values of these crucial parameters based on several independent (single molecule and cell-based) characterizing experiments. Using our model and independent derivation of the parameter values in conjunction with Monte Carlo simulations, we describe the binding of nanocarriers to endothelial cells at equilibrium. We show that we can quantitatively reproduce the experimental binding affinities with zero fitting to binding data. Additionally, our simulations provide quantitative descriptions for the multivalency in nanocarrier binding, as well as for the degree of clustering of antigens. Our study identifies two interesting parameters: glycocalyx resistance and antigen flexural rigidity both of which reduce binding of nanocarriers and alter the sensitivity of the nanocarrier binding constant to changes in temperature. Collectively, our model, parameter estimations, simulations, and sensitivity analyses help provide unified molecular and energetic analyses of the nanocarrier binding process.

Key Words: nanocarrier, glycocalyx, Monte Carlo, targeted drug delivery, endothelial cells

1. INTRODUCTION

Targeted drug delivery using functionalized nanocarriers offers many benefits lacking in conventional drug delivery systems, among which are improved efficacy and reduced toxicity [1]. Of many available technologies, targeting of therapeutic agents to the endothelial cells via specific receptor-mediated adhesion (such as through intercellular adhesion molecule-1 or ICAM-1), leads to enrichment of specificity [2, 3].

Several models have been proposed for the treatment of receptor-mediated adhesion of cells [4-7]. These models typically include the effects of receptor-ligand interaction strength, receptor and ligand densities, arrest/mobility of receptors/ligands on their respective surfaces, effects of membrane-mediated adhesion, etc., and have been successfully applied to neutrophil adhesion under uniform shear flow conditions [6]. Pioneering work by Bell [4, 5] on cell-cell adhesion laid the basic framework for much of the subsequent work in this field. In the Bell model, the specific attraction due to receptor-ligand bond formation is considered as a function of bond-length. Subsequent work by Hammer [6-8] on the simulation of the adhesive behavior of neutrophil (treated as rigid spheres), with randomly distributed receptors, in near contact with a planar endothelium under shear flow, identified several regimes of rolling and arrest behavior of neutrophil and delineated a state diagram. Following this body of work, we focus here on developing a physically-based coarse-grained model for accurate *in silico* predictions of functionalized nanocarriers binding to endothelial cells cultured *in vitro*. We propose a viable procedure for integrating a large number of system parameters that affect the binding process including the effect of the endothelial glycocalyx layer representing a thermodynamic barrier to the nanocarrier adhesion, which thus far, has not been considered in prior works.

Glycocalyx is a carbohydrate-rich zone on the cell exterior, mainly consisting of glycoproteins and proteoglycans [9, 10]. Its presence on the endothelial cell surface has been shown to have an effect on the binding of nanocarriers. Although models are available to represent mechanical properties of glycocalyx [11, 12], to our knowledge, a thermodynamic model which quantitatively predicts the effect of glycocalyx on nanocarrier binding is not available. However, *in vivo* experimental data of Mulivor [13] strongly suggests that the (partial) removal of glycocalyx by enzymatic (heparinase-mediated) degradation strongly influences nanocarrier binding [13]. In this study, the authors infused the femoral vein of rat with a rat anti-ICAM-1 functionalized nanocarrier solution. To mimic the effect of glycocalyx removal, the venules were perfused with the heparinase enzyme solution. The authors recorded the transient number of bound nanocarriers using fluorescence microscopy in presence and absence of glycocalyx and observed that the removal of glycocalyx increases the number of bound

* Honoring Keith E. Gubbins

† Corresponding author email: rradhak@seas.upenn.edu

nanocarriers by at least two-fold (see Figure 2). These studies highlight the importance of considering the contributions of the glycocalyx layer in constructing an accurate model for nanocarrier binding.

In this work, we consider three physical parameters, namely, glycocalyx resistance, flexural rigidity of receptors, and receptor-ligand bond-stiffness, in mediating nanocarrier adhesion to endothelial cells and strive to construct a microscopic model capturing these important physical characteristics (see our schematic in Figure 1). We develop rigorous procedures to estimate the parameter values of our model using independent experimental results reported in the literature, thus adopting a zero-fit approach. We then subject our model and simulation results to a rigorous test by comparing the predicted theoretical results with experimental results reported recently by Muro et. al. for the nanocarrier binding affinity to endothelial cells [14]. These authors investigated anti-ICAM (R6.5) functionalized polystyrene nanocarriers binding to HUVEC (human umbilical vein endothelial cells) at 4^0C under the conditions of cell fixation as well as stimulation by TNF-α. Finally, we provide results for parameter sensitivity in order to assess the role and importance of some key physical model parameters in governing the nanocarrier binding characteristics.

2. MODELS AND METHODS

2.1 Models

A schematic of our microscopic model for nanocarrier binding to endothelial cell is depicted in Figure 1. The largest length-scale considered in our model is that of the cell surface (~μm). In contrast, the relevant length-scale for interaction between proteins and ligands is ~10 nm. The 2-orders of magnitude separation in length-scale forbids us to employ an atomistically detailed description for our system and warrants the use of coarse-grained models and simplifying assumptions.

Following the work of Hammer et. al. [7, 8], we approximate the confluent endothelial cell surface by a planar non-deformable surface (a possible procedure for relaxing this assumption is given in section 4), while the polystyrene nanocarriers employed in the experiments of Muro [14] are modeled as rigid (hard) spheres. The nanocarrier is functionalized using antibodies specific to target antigens on the cell surface. Specifically, we consider the R6.5 antibody specific for ICAM-1 antigens in order to compare our model predictions with experiments [14] performed on the same system. In our model, the antibodies are distributed randomly, i.e. in random orientation at random positions, consistent with the experimental hydrophobic association protocol of Muro et al. [14] used to functionalize the nanocarrier surface (see Fig. 1). The antigens are in a vertical orientation (i.e. perpendicular to the cell surface) in their minimum energy configuration when unbound, and distributed randomly on the planar cell surface. Antigen flexure about this minimum energy configuration is also accounted for in our model, (see below).

Antigen-Antibody Interaction: In our model, the antigen-antibody bond-energy depends on the bond-length as well as the bond-orientation. For the dependence of reaction free energy on the bond-length, the Bell model [5] is employed, according to which the binding free energy ΔG is a quadratic function of the bond-length L with a minimum at the equilibrium value of the bond length σ, i.e.

$$\Delta G(L) = \Delta G(\sigma) + \tfrac{1}{2} k(L-\sigma)^2. \qquad (1)$$

Here, ΔG(σ) is the free energy of the reaction when the bond is at the equilibrium separation, σ. ΔG(L) is the free energy of reaction at bond length L, and k is the bond stiffness constant or bond spring constant.

Antigen Flexure: Flexure of antigens from their equilibrium upright position on the cell surface leads to an orientational dependence of the bond-energy. Considering small flexures, we model each antigen as a cantilever, and thus its contribution to the bond-energy ΔG due to flexure is equal to $(2EI/L^3)y_L^2$ (see Appendix A1), where y_L is the difference in the vertical distance of the tip of the bent antigen and that of an upright antigen, EI is the flexural rigidity (defined as the product of the Young's modulus E and the moment of inertia I), and L is the length of the antigen. Antibody flexure is not considered in our model.

Weinbaum *et. al.* [12] estimate the flexural rigidity EI for a glycoprotein to be 700 pN-nm^2, i.e. 7×10^{-28} N-m^2. By using this value for EI along with the length of ICAM-1 (L=19 nm [15] inferred from electron microscopic study), we calculated the bending energy for ICAM-1 for small deflections: $U(y_L) = \dfrac{2EI}{L^3} y_L^2 = 2.04\times10^{-4} y_L^2$, where $U(y_L)$ is in joule and y_L is in meter; y_L is the distance of the tip from its equilibrium position.

Glycocalyx Resistance: As the nanocarrier approaches the cell surface, it encounters resistance due to the presence of the glycocalyx layer (see Figure 1). Based on the biophysical characterization data of Squire et al. [16], we assume a height of 100 nm for the glycocalyx layer. The resistance offered by the glycocalyx layer, in

general, comprises of a combination of osmotic pressure (desolvation or squeezing out of water), electrostatic repulsion, steric repulsion between the nanocarrier and the glycoprotein chains of the glycocalyx, and entropic forces due to conformational restrictions imposed on the confined glycoprotein chains. We lump these effects into a single term of mechanical resistance due to glycocalyx by assuming a harmonic potential of the form $\frac{1}{2}k_{glyx}H^2$ per unit differential area, where 'H' is the penetration depth of the nanocarrier into the glycocalyx. Here, k_{glyx} can be regarded as an effective stiffness constant per unit area that effectively incorporates the molecular interactions described above. This additional resistance enters into thermodynamic considerations in calculating the Gibbs free energy change of binding. Specifically, for the binding of the nanocarrier to the cell, we get:

$$\Delta G(H) = \Delta G(0) + \iint \tfrac{1}{2} k_{glyx} H^2 dA, \qquad (2)$$

where, $\Delta G(0)$ is the free energy of the system when no glycocalyx is present on endothelial cells, and the integration is over the area of nanocarrier that is immersed in the glycocalyx.

2.2 Parameter Estimation

Based on the experiments of Muro [14] for free R6.5 (antibody) binding to free ICAM-1, $\Delta G(\sigma)$ is estimated to be -7.9×10^{-20} J/molecule at 4^0C. Consistent with the reported trend from the investigation of the temperature effects on the thermodynamic interaction between hen egg white lysozyme and Fab D1.3 antibody in a solvated environment for the temperature range 278 to 313 K by Zeder-Lutz [17], we assume that $\Delta G(\sigma)$ of the reaction is temperature-independent. In our model, the bond-spring constant k, and the equilibrium bond length σ, are also taken to be temperature independent (see section 3.3 for further comment on these assumptions). We calculate k_{glyx} based on the *in vivo* experimental data of Mulivor (described in the introduction) [13]: assuming that the nanocarrier binding is a second order reaction with respect to free nanocarriers and free antigens, and unbinding is a first order reaction for the bound-complex, we have shown in Appendix A2 that the concentration of bound nanocarriers as a function of time, C(t), is given by:

$$C(t) = k_f B C_{max}/(k_f B + k_r)\times[1-\exp[t(k_f B + k_r)]. \qquad (3)$$

Here, k_f and k_r are the forward and reverse rate constants, respectively, B is the concentration of free nanocarriers in solution, and C_{max} is the maximum concentration of nanocarriers that can bind to the cell-surface. By importing the values of B and C_{max} from the experiments of Mulivor et al., we regress k_f and k_r to fit the expression in Eq. (3) to the experimental data in Ref. [13], both in the presence of and in the absence of the glycocalyx, (see Figure 2 and Appendix A2). Using the inferred values of k_f and k_r, we compute the equilibrium constant K in the presence and in the absence of glycocalyx. The difference between $k_B T \ln K$ in the presence and absence of glycocalyx yields the change in the reaction free energy due to glycocalyx, i.e., $\Delta G(H) - \Delta G(0)$, in Eq. (2). The value of the glycocalyx spring constant k_{glyx} (reported in Table 1) is then determined from Eq. (2), see also Appendix A2.

Following Evans and Ritchie [18], we derive the dependence of the antigen-antibody bond rupture force f (described by the Bell model [5]) on force-loading rate r_f as given by:

$$f\times r_f/(k_B T) = k k^0 \exp[f^2/(2k)], \qquad (4)$$

where, k^0 is the unstressed bond-dissociation rate and k is the bond-spring constant. Fitting the above expression to the force-spectroscopy data of Moy et. al. [19] gives k^0 and k, (see Appendix A3).

2.3 Monte Carlo Protocol

A stochastic scheme based on the Metropolis Monte Carlo method [20] is developed for simulating the antibody (R6.5) functionalized nanocarrier binding to endothelial cells expressing antigens (ICAM-1) on the surface based on our model depicted in Figure 1. Periodic boundary conditions are enforced along the cell surface and impenetrable boundaries are enforced in a direction normal to the cell surface. The choice of boundary conditions is chosen for computational convenience and is not expected to impact the results with any significance. A summary of the system parameters is provided in Table 1.

Steric interactions between nanocarriers and antigens are considered through hardcore potentials (i.e., they are treated as hardspheres and hardrods, respectively). This simplifies our treatment of multicarrier simulations without introducing any significant artifacts because the density of nanocarriers and of the surface antigens are still significantly low and surface coverages we explore in our simulations (and in the experiments) are very much in the dilute limit so that interparticle interactions are not important. Still, it may be worthwhile to investigate the sensitivity of our results to the short-range potential of protein-protein interaction. This can be accomplished by calculating the potential of mean force between two membrane-bound antigens using atomistic or coarse-grained molecular dynamics simulations and to incorporate the effects of van der Waals, electrostatics, and hydrogen bond interactions, explicitly.

During each step of the Monte Carlo simulation, (which is based on the Metropolis algorithm [20]), one of the following actions are attempted to generate new system configurations for the nanocarrier or the surface

antigen: a nanocarrier is randomly selected and it either rotated or translated by a randomly chosen extent along a randomly chosen direction. If antigen diffusion is allowed in our model, then a randomly selected antigen is translated (on the cell-surface) by a random extent. The new system configuration is accepted with a probability: $\min[1, \exp(-(U_{new}-U_{old})/k_BT)]$, where k_B is the Boltzmann constant, T is the temperature in Kelvin scale, U_{new} and U_{old} are the potential energies of the new and old configurations, respectively, and the min operator selects minimum of the two values. The energy, U arises due to the hardsphere potential term or the glycocalyx resistance term. Whenever an antibody reaches within the bonding distance of an antigen, an additional step of bond-formation or bond-breakage is considered. A bond is formed between a randomly selected antigen and antibody within the bonding distance with a probability: $\min[1, \exp(-\Delta G/k_BT)]$. If the selected antigen and antibody pair is already bonded, then the bond is broken with a probability: $\min[1, \exp(\Delta G/k_BT)]$, where, ΔG is the change in energy due to formation of bond at given length and orientation . These calculations are performed 500 million times to ensure that properties such as total energy and multivalency converge. The results are reported here as an average over four independent simulations, each with 0.5 billion Monte Carlo steps. The error bars are reported as the standard deviation resulting from the four independent simulation runs.

3. RESULTS

3.1 Model Predictions and Comparison with Experiment

We perform simulations of nanocarrier adhesion to endothelial cells to make contact with the experimental work of Muro *et. al.* [14]. Consistent with their report, we choose the antigen density value of 1.6×10^6 antigens per endothelial cell. However, in converting this value to surface density of antigens in units of antigens/μm^2, we consider the uncertainty in the reported endothelial cell surface-area [21], namely, 800 to 2500 μm^2 per cell. We present our results for the two extreme values of the resulting antigen surface densities: 2000 and 640 antigens/μm^2.

Our results from simulations performed at 4^0C for the case of the antigens not allowed to diffuse on the cell surface (to mimic the scenario in fixed cells) are reported in Table 2 in which the multivalency calculated as the average number of antigen-antibody bonds formed per bound nanocarrier and the average binding energy of the nanocarrier binding are reported. For the range antigen and antibody densities we consider there is on an average two bonds per attached nanocarrier. However, owing to the bond-stretching the (negative) binding free energy of the nanocarrier (-14.5 to -16.7 kcal/mol) is considerably greater than -23 kcal/mol, which is twice the equilibrium binding free energy of the antigen-antibody interaction, (see Table 1). Using a Scatchard analysis of the experimental binding data [14], Muro et al. report an equilibrium dissociation constant K_D=77 pM for nanocarrier adhesion. This experimentally determined value of the binding affinity amounts to an equilibrium binding free energy of $\Delta G = -12.82$ kcal/mol, here we have used the relationship, $K_D=\exp(\Delta G/k_BT)$. Considering that our modeling results of the binding energy are obtained without direct fitting to nanocarrier binding data, we conclude that the agreement between simulations (Table 2) and experiment (−12.82 kcal/mol) is very favorable.

In order to consider the effect of surface diffusion of antigens on nanocarrier binding, we also performed simulations allowing the antigens to diffuse (Table 3). Not surprisingly, we find that allowing the surface antigens to diffuse in our simulations leads to increases in the multivalency as well as the binding affinity (i.e., a corresponding decrease in the negative binding energy) of nanocarrier binding, see Figures 3 and 4. In order to further establish the relationship between diffusing surface antigens and enhanced multivalency/binding energy, we map the in-plane 2-dimensional radial distribution function [20] related to the spatial distribution of surface antigens in our simulations in Figure 5. The radial distribution function is defined as the probability of finding two antigens at a given separation relative to the same probability if the antigens were completely randomly distributed. At a given separation, the radial distribution function value of greater than one indicates clustering of antigens at that separation. As evident from Figure 5, the ICAM-1 antigens cluster within a separation of 50 nm, which corresponds to the size (radius) of the nanocarriers. Moreover, as evident from the comparison of the radial distribution function plots in the presence and absence of the nanocarrier, the ICAM-1 clustering is clearly mediated by nanocarrier adhesion. These observations establish that the enhancement of multivalency and reduction of binding energy associated with the bound nanocarrier due to the diffusion of surface antigens is clearly mediated by antigen clustering.

3.2 Parameter Sensitivity to Model Predictions

In order to dissect the effect/sensitivity of the various physical components in our model on the binding characteristics of nanocarriers, we have performed additional simulations by varying key parameters, namely the bond stiffness constant and the flexural rigidity, over a range of 3 orders of magnitude. We report our results of this sensitivity analysis both in the presence and in the absence of glycocalyx in Figures 6 and 7. The effect of increasing the bond-stiffness constant (Figure 6) is to decrease the multivalency and increase the (negative) binding energy of nanocarriers (at a rate that is steeper than a linear dependence). The presence of glycocalyx

does not affect the multivalency but increases the binding energy. Interestingly, the difference in binding energy with and without glycocalyx is constant for all values of the bond-stiffness constants explored. The effect of varying the flexural rigidity on the multivalency and binding energy is similar to that we observe for the effect of the bond-stiffness constant (compare Figures 6 and 7): i.e., multivalency decreases and binding energy increases with increasing flexural rigidity and the presence of glycocalyx does not affect the multivalency but increases the binding energy for each value of the flexural rigidity. Again, the difference in the binding energy in the absence and presence of the glycocalyx is constant to a statistical significance for all values of the flexural rigidity we have explored. The dependence of the binding characteristics on the two parameters (namely the bond-stiffness constant and the flexural rigidity) we have uncovered provides new insight into the molecular parameters governing nanocarrier binding and establishes that these parameters act independently of the glycocalyx in mediating the binding equilibrium.

3.3 Role of Glycocalyx in Mediating Temperature Effects of Nanocarrier Binding

At equilibrium, the change in the Gibbs free energy of a process is related to its dissociation constant by the relationship, $\Delta G = RT \ln K_D$. In our model (see section 2.2 for a rationale), ΔG is temperature independent[‡] and hence, $\frac{d}{dT}\left(\ln K_D\right) = -\frac{\Delta G}{RT^2}$: this expression indicates that the magnitude and sign of ΔG determines the dependence of $\ln K_D$ with temperature. Since ΔG is usually a negative quantity for receptor-ligand interactions (with the exception of some active processes requiring metabolism [22]), the binding decreases with increasing temperature. In the mean-field limit (approximation) [23] for binding of nanocarriers, the overall free energy change can be represented as additive contributions of several terms: $\Delta G = \Delta G_{bonding} + \Delta G_{glyx} + \Delta G_{flex}$, where ΔG is the overall change in the free energy of the process, $\Delta G_{bonding}$ is change in free energy due to antigen-antibody bond-formation, ΔG_{glyx} is the free energy required to overcome glycocalyx resistance and ΔG_{flex} is the free energy contribution due to antigen flexure. Note that ΔG_{glyx} is positive, while $\Delta G_{bonding}$ is negative. Hence, the presence of glycocalyx is expected to alter the temperature dependence of the equilibrium dissociation constant for binding, K_D. That is, the temperature dependence of binding of nanocarriers to cells depends not only on the free antigen-antibody binding free energy, but also on endothermic terms such as the glycocalyx resistance (and perhaps the antigen flexural rigidity).

By carrying out simulations of binding at different T, we observe the expected effect of increase in the equilibrium dissociation constant with increase in temperature (Table 4). Intriguingly, we predict that this increase in the equilibrium dissociation constant of the nanocarrier with increase in temperature gets smaller with increase in glycocalyx resistance (see Table 4 and Figure 8). However, with respect to quantitatively capturing the temperature dependence in our model, we issue the following cautionary note: even though, we have developed rational procedures for estimating the key parameters of our model there is in general a need for more characterizing biophysical experiments to relieve the additional assumptions we have made, especially with respect to temperature dependence. For example, in our current model, the receptor-ligand complex bond spring constant is assumed to be temperature independent due to the lack of any supporting experimental data. Single molecule AFM experiments conducted over a limited temperature range suggests temperature softening of proteins [24], however, similar studies on protein-protein complexes are not yet available. In the future, such experiments would furbish the requisite temperature corrections to the bond-spring constant. Similarly, there is a growing need for independent characterizing biophysical experiments on antigen flexure and glycocalyx resistance for a enhancing the accuracy predictions relating to temperature effects.

4. DISCUSSION AND CONCLUSIONS

We describe an equilibrium model (Figure 1) for quantifying the effect of glycocalyx in mediating the interaction of functionalized nanocarriers with endothelial cells. Rather than fitting model parameters to

[‡] We note that in traditional thermochemistry of gas and aqueous phase reactions, we substitute $\Delta G = \Delta H - T\Delta S$ and assume that ΔH and ΔS are temperature independent, to get $\frac{d}{dT}\left(\ln K_D\right) = -\frac{\Delta H}{RT^2}$. However, in biomolecular reactions, these assumptions may not be generally valid due to a coupling of conformational and chemical degrees of freedom, and due to competing solvation and hydrophobic effects.

reproduce experimental binding data of nanocarriers to cells, we have described several new strategies (Appendices A2, A3, Figure 2, and Table A3-1) for a rational parameter estimation based on independent (single molecule and cell-based) characterizing experiments reported in the literature. This rational approach enables us to not only predict experimental binding constants of nanocarriers to endothelial cells without directly fitting to the binding data (Figures 3,4,6,7 and Tables 2,3), but also enables us to transfer the parameter values across similar systems.

We have shown that we can quantitatively reproduce the experimental binding affinities in a regime where the multivalency of nanocarrier is small (~2). The favorable agreement between simulations and experiment also validates our simplifying assumptions, however, we note that experiments under which high multivalency of nanocarriers (e.g., by increasing antibody density on the nanocarrier surface, or by replacing rigid nanocarriers by filomicelles) would provide a more rigorous test for our model assumptions, for a recent review, see Kane [25]. Our simulations provide quantitative descriptions for the multivalency in nanocarrier binding (Figures 3,6,7), as well as for the degree of clustering of antigens (Figure 5). Such a clustering of antigens is also suggested based on indirect inferences by Muro *et. al.* [26] in their experiments of nanocarrier adhesion to live endothelial cells. A more direct experimental validation of the clustering of ICAM-1 may be obtained via fluorescent labeling and fluorescence microscopy. Our study also identifies two interesting parameters (see further discussion below): glycocalyx resistance and antigen flexural rigidity, both of which reduce binding of nanocarriers and alter the sensitivity of the nanocarrier binding constant to changes in temperature. Both these parameters are physical and can be controlled experimentally: properties of the glycocalyx can be altered either by controlled cross-linking or by controlled enzymatic (heparinase) degradation, while the flexural rigidity of the antigens can be re-engineered by designing suitable mutant receptors. We suggest that for studying the effects of temperature on nanocarrier binding and testing our predictions in Table 4, the ideal experimental setup nanocarriers binding to fixed cells *in vitro* with arrested endocytosis between 4 and 37°C. These, used in combination with experiments using engineered systems to alter glycocalyx properties can directly validate our model predictions in Table 4 and Figure 8 with respect to the role of glycocalyx in altering the temperature dependence of nanocarrier binding to cells. A similar approach can be used to study the effect of antigen flexure on the temperature dependence of nanocarrier binding.

The interplay between different molecular and physical parameters often makes the results of biological experiments (such as nanocarrier binding to cells) difficult to analyze. By using our model, we have identified and dissected the effect of various parameters on the system's equilibrium behavior. The role of bond spring constant on carrier-binding to cells has been recognized by several researchers starting from the pioneering works of Bell [4, 5, 7, 8]. Our study here identifies two interesting new parameters, namely, glycocalyx resistance and antigen flexural rigidity, which are also important determinants of nanocarrier binding. The presence of glycocalyx effectively increases the binding free energy by repelling nanocarrier away from the endothelium surface without affecting the multivalency for binding. This conclusion is unaltered for the entire range of bond stiffness and flexural rigidities we have explored in our simulations (Figures 6,7). For this reason, the contribution from the glycocalyx is independent and uncorrelated from those due to the other parameters such as bond stiffness and flexural rigidity. We note that apart from this thermodynamic contribution, the presence of the glycocalyx significantly introduces several kinetic and hydrodynamic effects thereby likely altering the transient characteristics of nanocarrier binding which we have not considered here; for a brief review, see Weinbaum et al. [12].

The effect of antigen flexure can be understood by considering two competing effects: (1) antigen flexural rigidity reduces nanocarrier binding by effectively increasing the binding free energy (by an amount equal to the average strain energy due to flexure) in comparison to a freely flexing antigen. We note that the binding free energy is a negative quantity and an increase implies less binding. (2) However, in comparison to a rigid antigen, a flexing antigen allows for a better exploration of the conformational space and enhances multivalency. The net effect is an increase in binding affinity due an enhancement in the average number of receptor-ligand bonds. For the range of parameters we have explored, we find that upon increasing the flexural rigidity, the proportion by which the multivalency decreases translates quantitatively into the proportion by which the corresponding binding free energy increases, suggesting that the second effect dominates over the first (Figure 7). This behavior underscores the effect of flexural rigidity on nanocarrier binding and is unaltered in the presence or absence of glycocalyx. The analogous effect of varying the bond-stiffness (Figure 6) on the multivalency and binding energy has a subtle but important difference. In this case, while an increase in bond stiffness leads similarly to an overall decrease in multivalency and increase in binding free energy, the proportion by which the multivalency decreases does not quantitatively translate into (and is greater than) the proportion by which the binding free energy increases. This difference suggests that for the case of bond-stiffness, the analogous competing effects (1) and (2) are both important. This is a reflection of the fact that the role of strain energy associated with bond-stiffness in increasing the effective binding free energy is significantly greater than the corresponding role of the strain-energy due to flexure for the systems we have studied.

Even though we have focused on an equilibrium model and simulations, the model itself can as such be incorporated in a kinetic setting with minimal adjustments: for e.g., by replacing the Monte Carlo protocol by a Langevin dynamics protocol. Moreover, even though our study was focused on rigid spherical nanocarriers to make contact with the experiments of Muro et al. [14] using polystyrene nanospheres, there has appeared some very interesting recent data in the literature on the effect of nanocarrier size and shape [27, 28] and nanocarrier flexibility [28, 29] on binding properties. Extension of our model to treat rigid non-spherical nanocarriers is straightforward. However, including the effects of nanocarrier deformability in flexible carriers is more challenging. In this case, the choice of model integration would be dictated by the ratio of timescales: that associated with nanocarrier flexibility and that associated with the receptor-ligand binding reaction. This extension is also necessary for relaxing the assumption of the cell membrane surface as a planar rigid surface. In a live cell, membrane can undergoes undulations and a nanocarrier bound to live endothelial cell can additionally undergo endocytosis, which is preceded by membrane deformation and wrapping around the bound nanocarrier. Gao *et. al.* [30] have studied this problem in a model geometry (uniformly distributed antibodies and continuous density profile for antigens). As part of future work, we plan to combine our model discussed here along with a recent multiscale protocol [31] for membrane dynamics we developed in our laboratory in order to rigorously include the effects of membrane and carrier flexibility. Still, the simplified approach presented here, subject to the assumptions we have highlighted, qualifies as a predictive tool, and helps to provide a molecular resolution to the physico-chemical interactions and presents a unified molecular and energetic analyses of the nanocarrier binding process.

ACKNOWLEDGEMENTS

We thank Dr. Vladimir Muzykantov for providing us with the experimental details of R6.5 functionalized nanocarriers binding to ICAM-1 expressed endothelial cells and for many insightful discussions on the subject. We acknowledge funding from National Science Foundation through grant CBET-0730955 and from the Whitaker Foundation. Computational resources were available in part from the National Partnerships for Advanced Computational Infrastructure through grant MRAC MCB060006.

APPENDIX

A1: FLEXURAL RIGIDITY OF ANTIGENS

The energy stored in a beam due to a constant moment acting on it is given by $U = \frac{M^2 L}{2EI}$, where, M is the moment, L is the length of the beam and EI is the flexural rigidity of the beam. The deflection of a beam (oriented along x-axis with fixed end at the origin) is given by $\frac{d^2 y}{dx^2} = \frac{-M}{EI}$ [32]. For a constant M, we obtain, $y = \left(\frac{-M}{2EI}\right)x^2 + Ax + B$. To solve for A and B, we set $y(0) = 0$ and $y'(0) = 0$, and thus obtain $y = \left(\frac{-M}{2EI}\right)x^2$. Thus, the deflection of the free-tip is given by $y(L) \equiv y_L = \left(\frac{-M}{2EI}\right)L^2$. Substituting this result in the expression for the energy yields, $U(y_L) = \left(\frac{-2EIy_L}{L^2}\right)^2 \frac{L}{2EI} = \frac{2EI}{L^3} y_L^2$.

A2: FREE ENERGY CHANGE DUE TO GLYCOCALYX RESISTANCE

In this section, we represent a free nanocarrier as B, a free antigen on the cell as σ, and a bound nanocarrier as C. We can write the nanocarrier adhesion as a reaction (assuming each nanocarrier binds to one antigen only): $B + \sigma \rightleftharpoons C$; $\frac{dC}{dt} = k_f B\sigma - k_r C$; k_f and k_r denote the respective rates.

In a flow chamber experiment, the concentration of unbound nanocarriers is a constant. We can also express σ in terms of: $\sigma = C_{\max} - C$, where, $C_{\max}$ is the maximum concentration of nanocarriers that can bind

to the cell surface. Hence, $\frac{dC}{dt} = k_f B\left(C_{\max} - C\right) - k_r C$, with an initial condition of $C\left(t=0\right)=0$. We can integrate this differential equation to get:

$$C(t) = \frac{k_f B C_{\max}}{k_f B + k_r}\left\{1 - \exp\left(-\left(k_f B + k_r\right)t\right)\right\} \qquad \text{(A2-1)}.$$

In the work of Mulivor [13], B is specified in units of number of nanocarriers per mm^3, while C is specified as number of nanocarriers adsorbed per 100 μm of venule. We take volume of 100 μm of the venule as our unit-volume. Diameter of each venule is 39.5 μm, and so the volume per 100 μm of venule is 1.2254×10^{-4} mm^3. Hence, the units for B we have adopted and their relationship to the convention of Mulivor et. al. is provided in Table A2-1. From the results of Mulivor, we deduce that $C_{\max} = 180$ nanocarriers/100 μm of venule.

Hence, we fit the expression $C = \frac{k_f B C_{\max}}{k_f B + k_r}\left\{1 - \exp\left(-\left(k_f B + k_r\right)t\right)\right\}$ to the experimental data of Mulivor in the absence of glycocalyx to obtain k_f and k_r (Table A2-2). After removal of glycocalyx (t=30 min in the work of Mulivor), we can use the same rate equation, but with a slightly different initial condition: C(t'=0) = C_0, where, t'=t−30 min. We get,

$$C(t') = \frac{k_f B C_{\max}}{k_f B + k_r} + \left\{C_0 - \frac{k_f B C_{\max}}{k_f B + k_r}\right\}\exp\left(-\left(k_f B + k_r\right)t'\right). \qquad \text{(A2-2)}$$

After t=30 min, the glycocalyx is removed. We assume that the glycocalyx removal only changes (increases) the forward rate, k_f, while, k_r remains the same. By fitting the equations A2-1 and A2-2, we obtain $k_f\left(t<30\,\text{min}\right) = 500\times k_f\left(t>30\,\text{min}\right)$. This implies that the equilibrium constant in presence of glycocalyx is reduced by a factor of 500 relative to that in its absence, i.e., $K = 500K_{glyx}$. Hence,

$$\Delta G_{glyx} = \Delta G + k_B T \ln 500 = \Delta G + 2.573\times10^{-20}. \qquad \text{(A2-3)}$$

Within our harmonic model, the total resistance offered by the glycocalyx to nanocarrier adhesion is $E_{glyx} = \frac{1}{2}k_{glyx}\int\int\left\{z-\left(L-z_c\right)\right\}^2 dA$, (see figure 1 for nomenclature), where, the integration is over the area of nanocarrier that is immersed in the glycocalyx. The integral expressed in spherical coordinate system is:

$E_{glyx} = \frac{1}{2}k_{glyx}\int_{\phi_0}^{\pi}\int_{0}^{2\pi}\left\{\left(R\cos\phi\right)-\left(L-z_c\right)\right\}^2 R^2\sin\phi\, d\theta\, d\phi$, where, $\phi_0 = \cos^{-1}\left(\frac{L-z_c}{R}\right)$, and R is the hard sphere radius. The integral is solved to yield:

$$E_{glyx} = \frac{1}{2}k_{glyx}\left[\frac{2\pi R^4}{3}\left(\cos^3\phi_0+1\right)-2\left(L-z_c\right)\left(-\pi R^3\sin^2\phi_0\right)+\left(L-z_c\right)^2\left(2\pi R^2\left(\cos\phi_0+1\right)\right)\right],$$

which, upon further simplification gives,

$$E_{glyx}\left(z_c\right) = \pi R^2 k_{glyx}\left[\frac{R^2}{3}\left(\cos^3\phi_0+1\right)+R\left(L-z_c\right)\sin^2\phi_0+\left(L-z_c\right)^2\left(\cos\phi_0+1\right)\right]. \qquad \text{(A2-4)}$$

Equating $\Delta G_{glyx} - \Delta G$ in equation A2-3 to $E_{glyx}\left(z_c\right)$ in equation A2-4 allows us to estimate the value of k_{glyx} consistent with the experimental data of Mulivor et. al. This value for the glycocalyx spring constant (k_{glyx}) is provided in Table 1.

A3: FORCE SPECTROSCOPY

In force spectroscopy experiments, a constant/variable loading rate (force/time) is applied to the bonded antigen-antibody, and the time (i.e. force) at which bond ruptures is recorded [19, 33]. This experiment is repeated number of times to give rupture force distribution at a given loading rate.

From Evans [18], the probability of bond-rupture in a time interval $(t, t+dt)$ is given by:

$$p(t, f) = k_{off}(f)\exp\left(-\int k_{off}(f)dt\right). \qquad \text{(A3-1)}$$

The pre-factor represents the probability of dissociation in the next short interval of time, dt, whereas the exponential term represents the probability of the bond having survived up to time, t. We express $\Delta G(L) = -k_B T \ln K = -k_B T\left(\ln k_{on} - \ln k_{off}\right)$ using the Bell [5] model, as $\Delta G(L) = \Delta G(\sigma) + \frac{1}{2}k(L-\sigma)^2$. We assume that k_{on} is bond-length independent (since k_{on} is often diffusion-based; this assumption is consistent with Bell [4]). Hence, we obtain,

$$\Delta G(L) - \Delta G(\sigma) = k_B T \ln k_{off}(L) - k_B T \ln k_{off}(\sigma) = \frac{1}{2}k(L-\sigma)^2, \qquad \text{(A3-2)}$$

$$k_{off}(L) = k_{off}(\sigma)\exp\left(\frac{\beta}{2}k(L-\sigma)^2\right), \text{ i.e. } k_{off}(L) = k_{off}^0 \exp\left(\frac{\beta}{2}k(L-\sigma)^2\right). \qquad \text{(A3-3)}$$

Consistent with the harmonic approximation of Bell, $f = -k(L-\sigma)$. Using this definition in the above equation, we can express $k_{off}(L) = k_{off}^0 \exp\left(\frac{\beta}{2}\frac{f^2}{k}\right)$, and hence the probability as:

$$p(t, f) = k_{off}^0 \exp\left(\frac{\beta}{2}\frac{f^2}{k}\right)\exp\left(-\int k_{off}^0 \exp\left(\frac{\beta}{2}\frac{f^2}{k}\right)dt\right). \qquad \text{(A3-4)}$$

Expressing time in terms of the loading rate as $t = \frac{f}{r_f}$ yields:

$$p(f) = k_{off}^0 \exp\left(\frac{\beta f^2}{2k}\right)\exp\left(-\int k_{off}^0 \exp\left(\frac{\beta f^2}{2k}\right)\frac{1}{r_f}df\right). \qquad \text{(A3-5)}$$

The median of the probability distribution in Eq. (A3-5) is obtained by setting $\frac{d}{df}p(f) = 0$, i.e., $\frac{d}{df}\ln p(f) = 0$ to get $\beta f \times r_f = k \times k_{off}^0 \exp\left(\frac{\beta f^2}{2k}\right)$.

Hence, by fitting the equation to single molecule data, we can calculate bond-spring constant *k* and k_{off}^0. That is, we plot $x \equiv \beta f^2/2$ versus $y \equiv \beta f \times r_f$ to get bond-spring constant *k* and k_{off}^0 (see Table A3-1).

References

1. Khademhosseini, A.; Langer, R., Nanobiotechnology drug deliery and tissue engineering drug delivery and tissue engineering. *Chem. Eng. Prog.* **2006,** 102, 38.
2. Muro, S.; Muzykantov, V. R., Targeting of antioxidant and anti-thrombotic drugs to endothelial cell adhesion molecules. *Curr. Pharm. Des.* **2005,** 11, (18), 2383-401.
3. Sakhalkar, H. S.; Dalal, M. K.; Salem, A. K.; Ansari, R.; Fu, A.; Kiani, M. F.; Kurjiaka, D. T.; Hanes, J.; Shakesheff, K. M.; Goetz, D. J., Leukocyte-inspired biodegradable particles that selectively and avidly adhere to inflamed endothelium in vitro and in vivo. *Proc. Natl. Acad. Sci. U.S.A.* **2003,** 100, (26), 15895-15900.
4. Bell, G. I., Models for Specific Adhesion of Cells to Cells. *Science* **1978,** 200, (4342), 618-627.
5. Bell, G. I.; Dembo, M.; Bongrand, P., Cell adhesion. Competition between nonspecific repulsion and specific bonding. *Biophys. J.* **1984,** 45, (6), 1051-1064.
6. Bhatia, S. K.; King, M. R.; Hammer, D. A., The State Diagram for Cell Adhesion Mediated by Two Receptors. *Biophys. J.* **2003,** 84, 2671.
7. Hammer, D. A.; Apte, S. A., Simulation of cell rolling and adhesion on surfaces in shear flow: General results and analysis of selectin-mediated neutrophil adhesion. *Biophys. J.* **1992,** 63, 35.
8. Eniola, A. O.; Krasik, E. F.; Smith, L. A.; Song, G.; Hammer, D. A., I-Domain of Lymphocyte Function-Associated Antigen-1 Mediates Rolling of Polystyrene Particles on ICAM-1 under Flow. *Biophys. J.* **2005,** 89, (5), 3577-3588.

9. Pierres, A.; Benoliel , A.; Bongrand, P., *Cell-cell interaction*. Marcel Dekker: New York, 2000.
10. Robert, P.; Limozine, L.; Benoliel, A.-M.; Pierres, A.; Bongrand, P., *Glycocalyx regulation of cell adhesion*. Elsevier Academic Press: Amsterdam, 2006.
11. Chen, B.; Fu, B. M. M., An electrodiffusion-filtration model for effects of endothelial surface glycocalyx on microvessel permeability to macromolecules. *J. Biomech. Eng.-Trans. ASME* **2004,** 126, (5), 614-624.
12. Weinbaum, S.; Zhang, X.; Han, Y.; Vink, H.; Cowin, S. C., Mechanotransduction and flow across the endothelial glycocalyx. *Proc. Natl. Acad. Sci. U.S.A.* **2003,** 100, (13), 7988-7995.
13. Mulivor, A. W.; Lipowsky, H. H., Role of glycocalyx in leukocyte-endothelial cell adhesion. *Am. J. Physiol. Heart Circ. Physiol.* **2002,** 283, (4), H1282-1291.
14. Muro, S.; Dziubla, T.; Qiu, W.; Leferovich, J.; Cui, X.; Berk, E.; Muzykantov, V. R., Endothelial Targeting of High-Affinity Multivalent Polymer Nanocarriers Directed to Intercellular Adhesion Molecule 1. *J. Pharmacol. Exp. Ther.* **2006,** 317, (3), 1161-1169.
15. Kirchhausen, T.; Staunton, D. E.; Springer, T. A., Location of the Domains of Icam-1 by Immunolabeling and Single-Molecule Electron-Microscopy. *J. Leukocyte Biol.* **1993,** 53, (3), 342-346.
16. Squire, J. M.; Chew, M.; Nneji, G.; Neal, C.; Barry, J.; Michel, C., Quasi-periodic substructure in the microvessel endothelial glycocalyx: a possible explanation for molecular filtering? *J. Struct. Biol.* **2001,** 136, (3), 239-55.
17. Zeder-Lutz, G.; Zuber, E.; Witz, J.; Van Regenmortel, M. H. V., Thermodynamic Analysis of Antigen-Antibody Binding Using Biosensor Measurements at Different Temperatures. *Anal. Biochem.* **1997,** 246, 123-132.
18. Evans, E.; Ritchie, K., Dynamic strength of molecular adhesion bonds. *Biophys. J.* **1997,** 72, (4), 1541-55.
19. Zhang, X.; Wojcikiewicz, E.; Moy, V. T., Force Spectroscopy of the Leukocyte Function-Associated Antigen-1/Intercellular Adhesion Molecule-1 Interaction. *Biophys. J.* **2002,** 83, (4), 2270-2279.
20. Allen, M. P.; Tildesley, D. J., *Computer simulation of liquids*. Oxford science publications: Oxford, 1987.
21. Lomakina, E. B.; Waugh, R. E., Micromechanical tests of adhesion dynamics between neutrophils and immobilized ICAM-1. *Biophys. J.* **2004,** 86, (2), 1223-1233.
22. Marlin, S. D.; Springer, T. A., Purified Intercellular-Adhesion Molecule-1 (Icam-1) Is a Ligand for Lymphocyte Function-Associated Antigen-1 (Lfa-1). *Cell* **1987,** 51, (5), 813-819.
23. Chaikin, P. M.; Lubensky, T. C., *Principles of Condensed Matter Physics*. Cambridge University Press: Cambridge, 1995.
24. Schlierf, M.; Rief, M., Temperature Softening of a Protein in Single-molecule Experiments. *J. Mol. Biol.* **2005,** 354, (2), 497-503.
25. Kane, R. S., Polyvalency: Recent developments and new opportunities for chemical engineers. *AIChE J.* **2006,** 52, (11), 3638-3644.
26. Muro, S.; Wiewrodt, R.; Thomas, A.; Koniaris, L.; Albelda, S. M.; Muzykantov, V. R.; Koval, M., A novel endocytic pathway induced by clustering endothelial ICAM-1 or PECAM-1. *J. Cell Sci.* **2003,** 116, (8), 1599-1609.
27. Champion, J. A.; Katare, Y. K.; Mitragotri, S., Particle shape: A new design parameter for micro- and nanoscale drug delivery carriers. *J. Controlled Release* **2007,** 121, (1-2), 3-9.
28. Geng, Y.; Dalhaimer, P.; Cai, S.; Tsai, R.; Tewari, M.; Minko, T.; Discher, D. E., Shape effects of filaments versus spherical particles in flow and drug delivery. *Nat. Nanotechnol.* **2007,** 2, (4), 249-255.
29. Torchilin, V. P.; Lukyanov, A. N.; Gao, Z.; Papahadjopoulos-Sternberg, B., Immunomicelles: Targeted pharmaceutical carriers for poorly soluble drugs. *Proc. Natl. Acad. Sci. U.S.A.* **2003,** 100, (10), 6039-6044.
30. Gao, H.; Shi, W.; Freund, L. B., From The Cover: Mechanics of receptor-mediated endocytosis. *Proc. Natl. Acad. Sci. U.S.A.* **2005,** 102, (27), 9469-9474.
31. Weinstein, J.; Radhakrishnan, R., A coarse-grained methodology for simulating interfacial dynamics in complex fluids: application to protein mediated membrane processes. *Mol. Phys.* **2006,** 104, (22-24), 3653-3666.
32. Riley, W. F.; Sturges, L. D.; Morris, D. H., *Statics and mechanics of materials : an integrated approach*. John Wiley and Sons: New York, 1995.
33. Hanley, W.; McCarty, O.; Jadhav, S.; Tseng, Y.; Wirtz, D.; Konstantopoulos, K., Single molecule characterization of P-selectin/ligand binding. *J. Biol. Chem.* **2003,** 278, (12), 10556-10561.

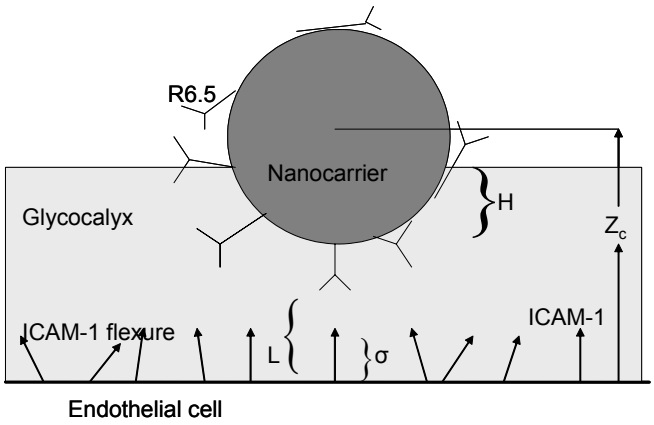

Figure 1: Schematic of the microscopic model for nanocarrier binding to endothelial cells.

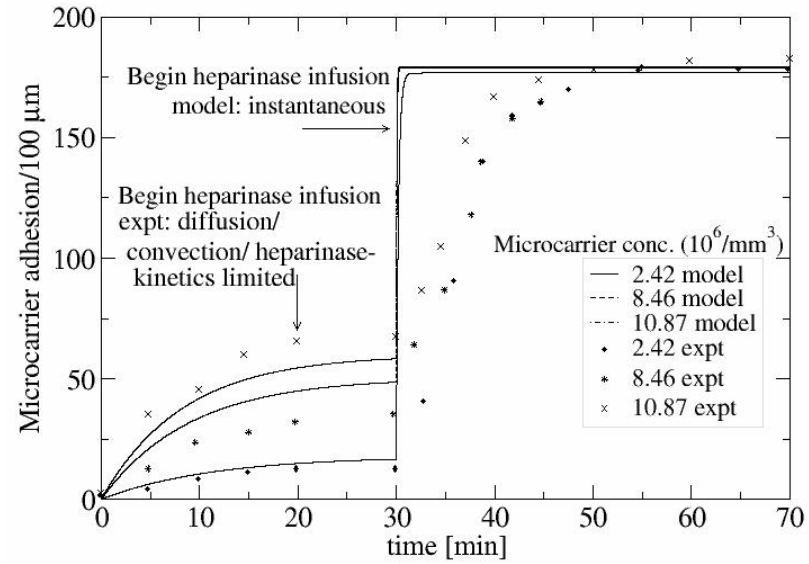

Figure 2: Regression of the glycocalyx model (Equations 3, and A2-2) to the experimental data of Mulivor [13] provides an avenue to estimate the glycocalyx sprint constant k_{glyx} reported in Table 1.

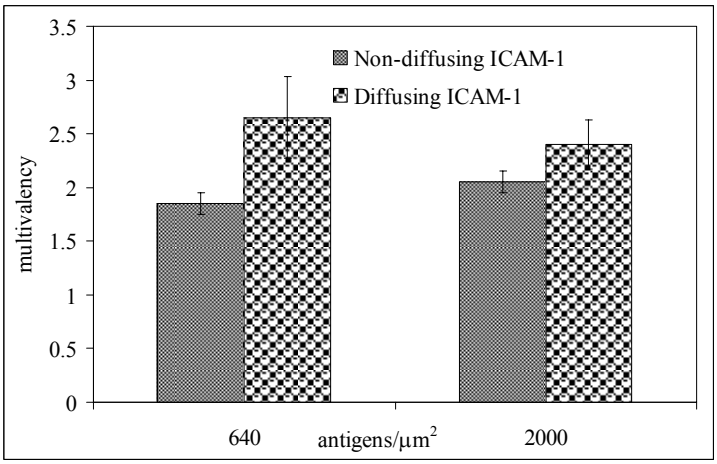

Figure 3: Effect of ICAM-1 diffusion on nanocarrier multivalency: a visual comparison of data from Tables 2 and 3.

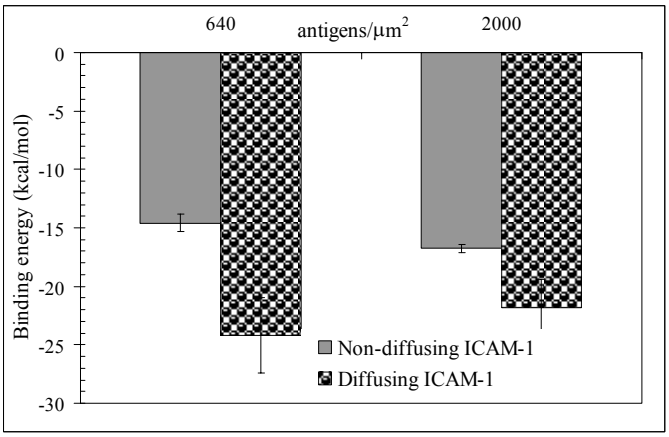

Figure 4: Effect of ICAM-1 diffusion on nanocarrier binding energy: a visual comparison of data from Tables 2 and 3.

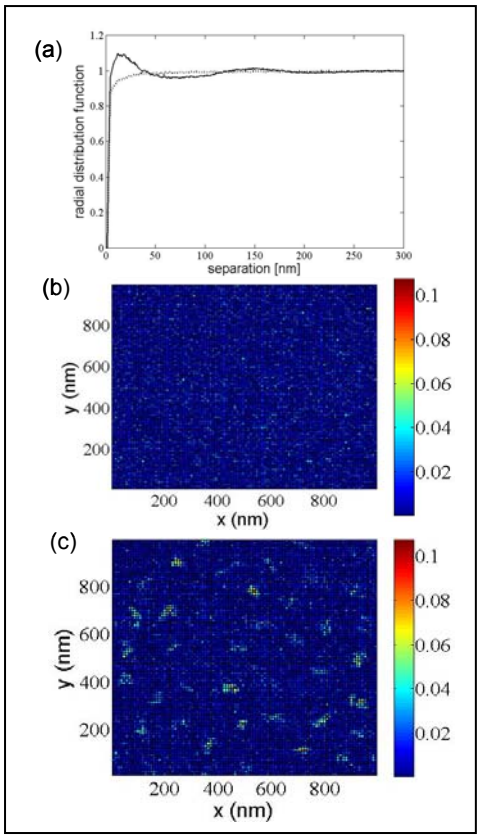

Figure 5: (a) Radial distribution function of diffusing antigens on the cell surface in the presence (solid line) and absence (dotted line) of bound nanocarriers. Simulations are performed with 640 antigens/μm^2 and 50 nanocarriers at 4^0C. (b) Percentage of probability of spatial occupancy of surface antigens in the absence of bound nanocarriers. (c) Percentage of probability of spatial occupancy of surface antigens in the presence of bound nanocarriers. A visual comparison of (b) and (c) clearly indicates clustering of antigens only in the presence of bound nanocarriers.

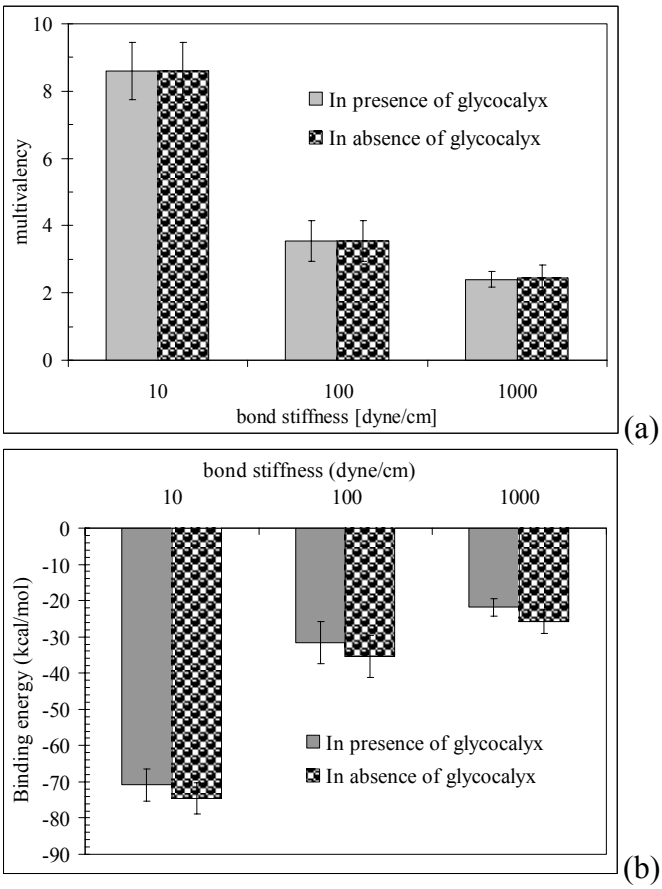

Figure 6: Effect of bond-stiffness (k) on nanocarrier (a) multivalency, and (b) binding energy for diffusing ICAM-1. Presence of glycocalyx does not affect the multivalency, though it increases the (negative) binding energy. Simulations are performed for 2000 antigens /μm^2.

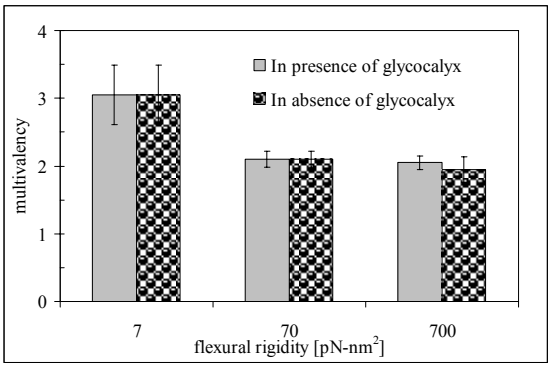

(a)

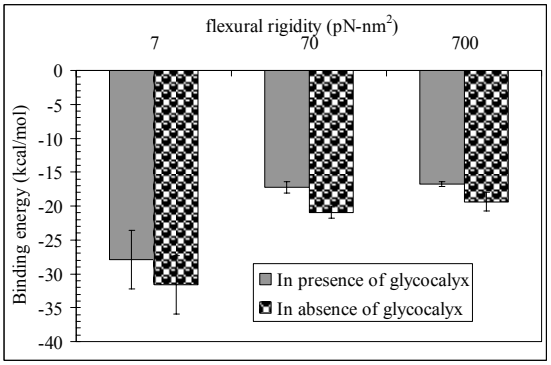

(b)

Figure 7: Effect of ICAM-1 flexural rigidity on nanocarrier (a) multivalency and (b) binding energy for non-diffusing ICAM-1. Presence of glycocalyx does not affect the multivalency, though it increases the (negative) binding energy. Simulations are performed for 2000 antigens /μm^2.

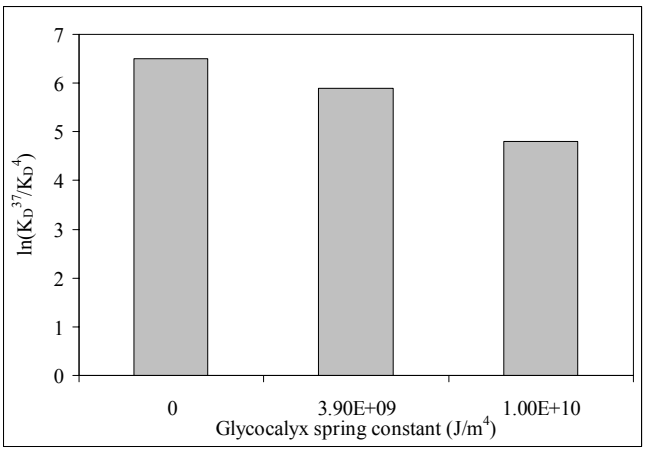

Figure 8: Difference of $\ln K_D$ of binding at 37^0C and 4^0C plotted against the glycocalyx spring constant k_{glyx}. The difference between $\ln K_D$ at 37^0C and 4^0C decreases with increasing glycocalyx resistance, thus reducing the temperature dependence of the binding process.

TABLE 1: System Parameters

Parameter	Value	Reference
Simulation cell area	1 μm^2	
Simulation cell height	0.5 μm	
Nanocarrier diameter	100 nm	
Antigen length	19 nm	[15]
Antibody length	15 nm	
Antigen/antibody radius	1.5 nm	
Number of antibodies per nanocarrier	220	[14]
$\Delta G(\sigma)$	-7.98×10^{-20} J	[14]
Bond spring constant	1000 dyne/cm	*[19]
Glycocalyx height	100 nm	[16]
Glycocalyx spring constant	3.9×10^{9} J/m^4	*[13]
Antigen flexural rigidity	700 pN-nm^2	[12]

*Estimated based on the experimental data

TABLE 2: Binding of nanocarriers to non-diffusing ICAM-1 on the endothelial cell surface: model predictions

Antigens/μm^2	Multivalency	Binding energy (kcal/mol)
640	1.85±0.1	-14.57 ± 0.72
2000	2.05±0.1	-16.75 ± 0.34

TABLE 3: Binding of nanocarriers to diffusing ICAM-1 on the endothelial cell surface: model predictions

Antigens/μm^2	Multivalency	Binding energy (kcal/mol)
640	2.65±0.4	-24.16 ± 3.22
2000	2.4±0.2	-21.82 ± 2.42

TABLE 4: Effect of glycocalyx on the nanocarrier dissociation constant

Glycocalyx spring constant (J/m^4)	$\ln K_D$*		ln ($K_D^{37°C}$ / $K_D^{4°C}$)
	4 °C	37 °C	
0	-94.4±3.5	-87.8±0.9	6.5
3.9×10^{9}	-87.74±3.6	-81.8±0.9	5.9
1.0×10^{10}	-77.34±3.6	-72.5±0.9	4.8

*Values reported for diffusing ICAM-1 and with flexural rigidity of 7 pN-nm^2

TABLE A2-1: Concentration of nanocarriers

B [10^6/mm^3]	B [# nanocarriers/100 μm of venule]
2.42	294.55
8.46	1036.69
10.87	1332.01

TABLE A2-2: Rate constants of nanocarrier binding reaction

B (# nanocarriers/100 μm of venule)	k_f *	k_r *
294.55	2.436×10^{-5}	0.08304
1036.69	1.897×10^{-5}	0.07393
1332.01	3.755×10^{-5}	0.07965
* Unit of k_f is [(#/100 μm of venule)×minute]$^{-1}$; unit of k_r is 1/min.		

TABLE A3-1: Fitting k to the experimental data of Zhang [19] and Hanley [33]

Antigen-Antibody pair	r_f pN/s	k (dyne/cm)	k_{off}^0 s^{-1}	r^2 *
ILFA-1/iICAM-1 [19]	20-10,000	1143.38	10.34	0.9955
hLFA-1/iICAM-1 [19]	20-10,000	1219.66	2.3	0.9989
ILFA-1/iICAM-1 w/EDTA [19]	20-10,000	484.5	8.475	0.9979
P-selectin/PSGL-1 [33]	100-10,000	2509.4	2.06	0.9987
P-selectin/LS174T [33]	200-5000	1310.44	5.86	0.9943
* Goodness of fit				